Journal of Medicinal Chemistry

Article

Manganese Complex of Ethylenediaminetetra acetic acid (EDTA)-Benzothiazole Aniline (BTA) Conjugate as a Potential Liver-Targeting MRI Contrast Agent

Md. Kamrul Islam, Soyeon Kim, Hee-Kyung Kim, Subin Park, Gang Ho Lee, Hyo Jeung Kang, Jae Chang Jung, Joon-Suk Park, Tae-Jeong Kim, and Yongmin Chang

J. Med. Chem., **Just Accepted Manuscript** • DOI: 10.1021/acs.jmedchem.6b01799 • Publication Date (Web): 16 Mar 2017

Manganese Complex of Ethylenediaminetetra acetic acid (EDTA)-Benzothiazole Aniline (BTA) Conjugate as a Potential Liver-Targeting MRI Contrast Agent

Md. Kamrul Islam,[1,‡] Soyeon Kim,[1, ‡] Hee-Kyung Kim,[2] Subin Park,[3] Gang-Ho Lee,[4] Hyo Jeung Kang,[5] Jae-Chang Jung,[3] Joon-Suk Park,[8] Tae-Jeong Kim,[6,] and Yongmin Chang,[1,2,7,*]*

[1]Department of Medical & Biological Engineering, [2]Department of Molecular Medicine & BK21 Plus KNU Biomedical Convergence Program, [3]Department of Biology, [4]Department of Chemistry, [5]Department of Pharmacy, [6]Institute of Biomedical Engineering Research, [7]Department of Radiology, Kyungpook National University, 80 Daehakro, Bukgu, Daegu 702-701, Korea, [8]Laboratory Animal Center, Daegu-Gyeongbuk Medical Innovation Foundation 41061, Chumbok-ro 80, Dong-gu, Daegu, Korea

KEYWORDS: Manganese, Contrast agent, MRI, Liver, Chelate

ABSTRACT: A novel manganese (II) complex based on an ethylenediaminetetraacetic acid (EDTA) coordination cage bearing a benzothiazole aniline (BTA) moiety (Mn-EDTA-BTA) was designed and synthesized for use as a liver-specific MRI contrast agent with high chelation stability. In addition to forming a hydrophilic, stable complex with Mn^{2+}, this new Mn chelate was rapidly taken up by liver hepatocytes and excreted by the kidneys and biliary system. The kinetic inertness and R1 relaxivity of the complex were much higher than those of mangafodipir trisodium (MnDPDP), a clinically approved liver-specific MRI contrast agent. The diagnostic utility of this new Mn complex in MRI was demonstrated by high-sensitivity tumor detection in an animal model of liver cancer.

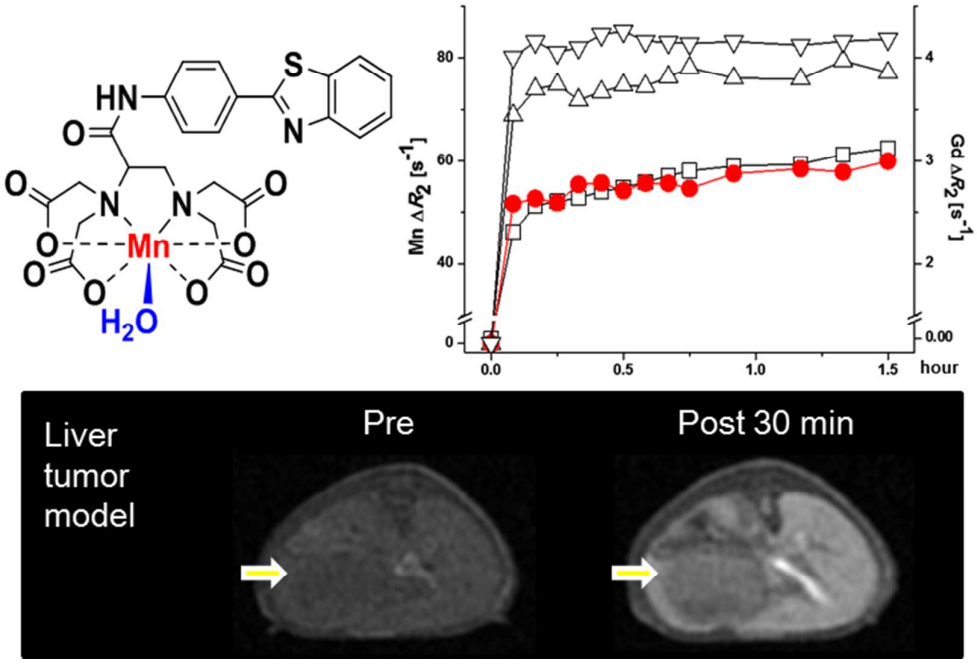

INTRODUCTION

Manganese (Mn) carries five unpaired electrons and is one of the earliest paramagnetic metal ions reported to effectively enhance positive contrast in magnetic resonance imaging (MRI).[1,2] As a clinical MRI contrast agent (CA), gadolinium (Gd) is mostly used. However, Gd-complex is linked with nephrogenic systemic fibrosis (NSF).[3,4] NSF is a rare, idiopathic systemic fibrosing disorder and can be critical to patients with acute or chronic kidney disease (CKD) with severely impaired renal function.[5] Furthermore, it has been recently reported that intravenously administered Gd accumulates in the brains of patients with normal renal function.[6] With increasing safety concerns over potential toxicities associated with Gd retention in the human body, alternative approaches based on non-lanthanide metals, particularly Mn, are receiving more attention for use in MRI.[7,8]

Mn plays a critical role in cell function.[9] It is a natural cellular constituent and is required for mitochondrial function. Hepatocytes are mitochondria-rich cells; thus, Mn is an excellent CA for MRI of the liver.[10] Although small amounts are essential in humans, overexposure to free Mn ions may result in neurotoxicity.[11] It has been known for many years that chronic exposure to Mn in certain occupational settings leads to a neurological syndrome known as manganism, which is similar to Parkinson's disease.[12] The neurological symptoms of manganism correlate with accumulation of Mn in the basal ganglia, which can often be seen as hyper-intensity on a T1-weighted MRI owing to contrast enhancement from the Mn accumulation.[13] Furthermore, although no association has been found between Mn and NSF so far, potential harmful effects of exposure to free Mn ions at a high concentration remain a concern with regard to its use as a CA. Indeed, MnDPDP (mangofodipir trisodium), which was approved by the FDA for use as a T1 MR CA for liver imaging, releases free Mn in

plasma after intravenous (IV) injection.[14] When an MRI dose (i.e. 5–10 mmol/kg) is injected into a human patient, only about 20% remains bound to the chelator. Release of paramagnetic Mn^{2+} occurs through dose-dependent transmetalation, in which Mn^{2+} is displaced by endogenous Zn^{2+}.[15] Zn^{2+} has roughly 1000 times higher affinity than Mn^{2+} does for DPDP. Free Mn^{2+} ions dissociated from MnDPDP are in fact responsible for the T1 contrast enhancement of MnDPDP.[16] Although free Mn^{2+} ions are known to accumulate primarily in the liver, pancreas, and heart, one report showed Mn^{2+} accumulation in patients' brains, suggesting possible neurotoxicity.[17]

Several efforts have been made to design stable Mn(II) complexes for MRI. Recently, Caravan et al. synthesized an Mn(II) complex of $[Mn(PyC3A)(H_2O)]^-$ as an alternative CA to Gd. This complex is one of the most stable Mn(II) complexes at pH 7.4 (log K_{ML} = 11.40) and has a possible application as a molecular agent for vascular thrombi.[18] More recently, Lattuada et al. synthesized a new Mn(II)-EDTA-deoxycholic acid conjugate as a potential MRI blood pool agent.[19] However, design of stable liver-specific Mn(II) complexes remains a challenge. In the current study, we report the design and synthesis of a new liver-specific, highly stable Mn chelate for liver MRI. Specifically, we designed a novel Mn(II) complex based on an EDTA coordination cage bearing a benzothiazole aniline (BTA) moiety with high chelation stability for use as a liver-specific MRI CA. BTA derivatives have high lipophilicity and sufficient protein-binding affinity.[20] We therefore hypothesized that BTA will contribute to the increased lipophilicity of Mn-EDTA-BTA, which will enhance its ability to target liver cells. In case of liver-specific Gd agents such as gadolinium dimeglumine ethoxybenzyl (Gd-EOB-DTPA), lipophilicity is known to enhance liver uptake.[21]

In addition to forming a hydrophilic, stable complex with Mn^{2+}, this new hepatobiliary Mn chelate is rapidly taken up by liver hepatocytes. We believe this complex is the first example of a small Mn-chelate-based liver agent with high *in vivo* stability. This new family of CAs is highly suitable for liver imaging applications such as liver cancer imaging.

RESULTS AND DISCUSSION

Synthesis. The methods for synthesis of the chelate conjugate and its Mn(II) complex (abbreviated as L and Mn-EDTA-BTA, respectively) are depicted in Scheme 1. Synthesis of the ligand, L started with the commercially available D,L-2,3-diaminopropionic acid monohydrobromide. Compound **1** was synthesized following a published method,[22] and was conjugated to BTA in the presence of triphenyl phosphite to form a white solid **2**. tert-butyl was cleaved using a mixture of trifluoroacetic acid (TFA) and dichloromethane, to yield a pale-yellow product **3** after precipitation. Alkylation with tert-butyl bromoacetate under conditions reported previously[23] resulted in a high yield of the protected EDTA-BTA compound **4** after column chromatography. After deprotection with hydrochloric acid, the ligand L was purified from the reaction mixture by precipitation at pH 2. The Mn complex Mn-EDTA-BTA was prepared by reaction of L with a stoichiometric equivalent of $MnCl_2.4H_2O$ at pH 6 followed by removal of inorganic impurities by reverse-phase chromatography. The pure chelate was isolated as a sodium salt in moderate yield by lyophilization. The formation of the ligand and its Mn-complex was confirmed by microanalysis and spectroscopic techniques including ^{1}H NMR, HR-FAB-MS and elemental analysis (Supporting Information).

Kinetic inertness. Zn is the second most abundant trace metal in the human body and can thus displace more Mn^{2+} ions than other endogenous ions such as Cu^{2+} and Ca^{2+}. The rate of

transmetalation of an Mn ligand chelate is inversely correlated with the stability of the complex. The relative stability of CAs can therefore be measured by determining the kinetics of their transmetalation with Zn^{2+}. Transmetalation rates are often represented by plotting the evolution of the normalized longitudinal (R1) or transverse (R2) relaxivity as a function of time.[24,25] In the current study, the kinetic inertness of Mn-EDTA-BTA is represented by a change in transverse relaxivity ($\Delta R2(t) = R2(t) - R2(0)$) as a function of time. Here, R2(t) at any time t is a good estimator of the extent of transmetalation of Mn by Zn. MnDPDP, Mn-EDTA, and Gd-DTPA were also examined for comparison (Figure 1). We prepared the complex under two conditions following a published method with slight modifications.[18] Transmetalation was evaluated by measuring $\Delta R2(t)$ of each Mn-EDTA-BTA complex incubated with Zn^{2+} (10 or 25 equivalents) in pH 6.0 MES buffer. The results were consistently similar in all cases, and a representative set is presented here (10 mM Zn^{2+}). The same method was used to evaluate transmetalation of MnDPDP, Mn-EDTA, and Gd-DTPA. The $\Delta R_2(t)$ of MnDPDP rapidly increased and reached saturation. In contrast, the $\Delta R_2(t)$ of Mn-EDTA-BTA rapidly increased at first, but subsequently slowed to reach saturation at a much lower $\Delta R_2(t)$ value compared to that of MnDPDP. Therefore, compared to MnDPDP, Mn-EDTA-BTA is significantly more inert to Mn^{2+} transmetalation. Figure 1 also shows that Mn-EDTA-BTA is kinetically more stable than Mn-EDTA is, suggesting the possible role of the BTA moiety in stabilizing Mn chelation. Furthermore, the pattern of $\Delta R_2(t)$ for Mn-EDTA-BTA is almost identical to that for Gd-DTPA, the widely used clinical MRI CA, indicating that Mn-EDTA-BTA is as stable as Gd-DTPA is.

Relaxivity and lipophilicity. The relaxivity values of Mn-EDTA-BTA are summarized in Table 1 along with those of MnDPDP, Mn-EDTA, and Gd-DTPA for comparison. Of the 3 complexes, Mn-EDTA-BTA had the highest relaxivity (Table 1). Although Mn^{2+} (S=5/2) has

fewer unpaired electrons than Gd^{3+} (S=7/2) does, the lipophilic moiety BTA has a slower tumbling rate and might contribute to high relaxivity relative to that reported for Gd-DTPA or Mn-EDTA. In addition, the shorter distance between Mn^{2+} and water may contribute to the increased relaxivity of Mn-EDTA-BTA.[21] We also measured relaxivity in an aqueous solution of human serum albumin (HSA). In this solution as well, the relaxivity values of Mn-EDTA-BTA were higher than those of Gd-DTPA, and indicated an interaction between HSA and Mn-EDTA-BTA. The binding constant (K_a), reflecting the interaction of Mn-EDTA-BTA with HSA was determined following a previously published method.[26] The K_a of Mn-EDTA-BTA binding to HSA (95 M^{-1}) was higher than that of Gd-DOTA binding to HSA (21 M^{-1}).[27] Figure 2 shows the result of fitting data obtained by measuring the proton longitudinal relaxation rate as a function of the concentration of Mn-EDTA-BTA, at a fixed concentration of HSA. To estimate lipophilicity, we determined the octanol-water partitioning coefficient (logP). The logP value for Mn-EDTA-BTA (logP = -1.84) was higher than those of MnDPDP (logP = -3.07), Mn-EDTA (logP = -2.72), and Gd-DTPA (logP = -3.16), demonstrating the higher lipophilicity of Mn-EDTA-BTA (Table 1).

***In vitro* cytotoxicity.** Tests of Mn-EDTA-BTA and Gd-DTPA cytotoxicity were performed on the human prostate cancer cell line DU 145, and the mouse liver cell line NCTC 1469. Figure 3 shows that viability of DU 145 cells was above 88%, and that of NCTC 1469 cells was above 86% when incubated with various concentrations of Mn-EDTA-BTA up to 50 μM. As shown in Figure 3, Mn-EDTA-BTA showed lesser cytotoxicity than Gd-DTPA did at all concentrations. These observations indicate that Mn-EDTA-BTA has negligible cytotoxicity in the concentration range needed to sufficiently enhance signal intensity in MRI.

***In vivo* MRI and *in vivo* biodistribution.** *In vivo* MRI using Mn-EDTA-BTA was performed by obtaining T1-weighted MR images of 6-week-old male mice of the Institute for Cancer Research strain (ICR mice) after a bolus injection of Mn-EDTA-BTA through the tail vein (Figure 4). The most characteristic MR feature of Mn-EDTA-BTA is that it shows strong contrast enhancement in the liver and kidney after injection, and subsequently in the gallbladder and intestine as well. *In vivo* MRI therefore indicates that Mn-EDTA-BTA is eliminated via hepatobiliary and renal pathways. In the hepatobiliary pathway, Mn-EDTA-BTA is eliminated via the bile duct following hepatobiliary uptake. Interestingly, this dual elimination property of Mn-EDTA-BTA is similar to that of the clinically approved Gd-based liver-specific agent Gd-DTPA-EOB.[21] *In vivo* biodistribution of Mn-EDTA-BTA was quantitatively measured with an inductively-coupled plasma (ICP) spectrophotometer (Figure 5). The data show the highest Mn(II) accumulation in the liver and intestine, indicating Mn-EDTA-BTA excretion via the hepatobiliary pathway. In addition to the liver, the kidney shows relatively high Mn(II) accumulation, suggesting glomerular excretion via the renal pathway. Together with the MRI data, the *in vivo* biodistribution data strongly suggest that Mn-EDTA-BTA is eliminated via dual pathways (renal and hepatobiliary).

Hepatocyte targeting. Figure 6 shows stronger signal enhancement in the nucleus rather than at the plasma membrane or in the cytosol of NCTC 1469 cells (a normal mouse hepatocyte cell line), demonstrating the subcellular preferential targeting of Mn-EDTA-BTA. These experiments provide direct evidence that the liver MR signal enhancement is a result of hepatocyte targeting by Mn-EDTA-BTA. However, a further study is warranted to investigate the detailed mechanism of hepatocyte targeting of Mn-EDTA-BTA, although its lipophilicity may be partly responsible for this. In the case of Gd-DTPA-EOB, the active

transport system on the hepatocyte membrane plays an important role. Specifically, Gd-DTPA-EOB enters hepatocytes through two different organic anion transport systems.[21] In addition, in future studies, it will be important to identify more efficient alternatives to BTA, for hepatocyte targeting.

Tumor imaging: Distinction between normal liver and tumor tissue. Because Mn-EDTA-BTA behaves as a liver-specific agent, we performed an *in vivo* test to determine whether it can distinguish between normal and tumor liver tissue. Figure 7a and 7b show T2-weighted and T1-weighted MR images from a HepG2 xenograft mouse model before and after injection of Mn-EDTA-BTA or MnDPDP. T2-weighted images without CA injection clearly showed the tumor location and size. In the case of Mn-EDTA-BTA, greater signal enhancement is seen in normal liver tissue than in tumor tissue. However, in the case of MnDPDP, positive signal enhancement is seen in both normal liver and tumor tissue, suggesting that normal hepatocytes and tumor cells efficiently take up MnDPDP. Mn-EDTA-BTA thus showed a higher difference in contrast-to-noise ratio (ΔCNR) between tumor and normal liver tissue (Figure 7c) than MnDPDP did, suggesting a significant improvement in tumor detection and characterization. From the kinetic stability data (Figure 1), one possible mechanism for a significant improvement in contrast between tumor and normal liver tissue is that Mn-EDTA-BTA remains as a stable complex and thus is taken up only by normal liver cells. However, MnDPDP is dissociated into free Mn^{2+} ions and DPDP, and free Mn^{2+} ions enter all cells with equal efficiency, enhancing both tumor and normal liver tissue equally.

In summary, Mn-EDTA-BTA shows good potential as a diagnostic agent for liver cancer. It should be mentioned that although the injection dose of MnDPDP used in the current study

was lower than that of Mn-EDTA-BTA, based on the suggested clinical dose of MnDPDP,[28] the main reason for the low ΔCNR of MnDPDP between tumor and normal liver tissue was not the low dose but the uptake of MnDPDP both in tumor and normal liver tissue. Furthermore, the injection dose of MnDPDP could not be increased because of possible toxicity *in vivo*, especially due to neurotoxicity of Mn^{2+} released from DPDP.

CONCLUSIONS

In the current study, we synthesized and characterized an Mn-EDTA complex incorporating a BTA functionality, and investigated its possible diagnostic utility in liver MRI. The kinetic inertness of this complex was much higher than those of MnDPDP and Mn-EDTA, and was comparable to that of stable Gd-DTPA. Furthermore, its R1 relaxivity (3.47 mM^{-1} s^{-1}) was higher than those of MnDPDP (R1 = 2.8 mM^{-1} s^{-1}) and Gd-DTPA (R1 = 3.3 mM^{-1} s^{-1}). *In vivo* biodistribution and *in vivo* MRI patterns effectively demonstrated that Mn-EDTA-BTA is a liver-specific MRI CA that utilizes both renal and hepatobiliary elimination pathways. This elimination pattern is similar to that of Gd-based hepatobiliary agents such as Gd-DTPA-EOB and Gd-BOTPA. Finally, in an animal model of liver cancer, Mn-EDTA-BTA significantly improved tumor detection and characterization compared to that observed with MnDPDP, suggesting that Mn-EDTA-BTA may be a good diagnostic MRI agent for liver cancer.

EXPERIMENTAL SECTION

General remarks. D,L-2,3-diaminopropionic acid monohydrobromide, di-*tert*-butyl dicarbonate, triphenyl phosphite, N,N-diisopropylethylamine, and ethylenediaminetetraacetic acid manganese disodium salt hydrate (Mn-EDTA) were purchased from Tokyo Chemical Industry (Tokyo, Japan). *tert*-Butyl-bromoacetate was obtained from Alfa-Aesar (Ward Hill, Massachusetts, USA). Sodium bicarbonate ($NaHCO_3$) was purchased from Daejung Chem. (Korea). Potassium iodide (KI) and sodium sulfate (Na_2SO_4) anhydrous were purchased from Duksan Scientific Corp. (Korea). All other commercial reagents were purchased from Sigma-Aldrich (St. Louis, MO, USA) and used without further purification unless otherwise stated. Solvents were purified and dried using standard procedures. Deionized water was used for all experiments. ^{1}H NMR spectra was recorded on a Bruker Advance 500 MHz spectrometer at the Center for Instrumental Analysis, Kyungpook National University (KNU). Chemical shifts are given as δ values with reference to tetramethylsilane (TMS) as the internal standard. Coupling constants are in Hz. Elemental analyses (EA) were performed by the Center for Instrumental Analysis, KNU. High-resolution fast atom bombardment mass spectra (HR-FAB-MS) were obtained using a JMS-700 model (Jeol, Japan) mass spectrophotometer at the Korea Basic Science Institute (KBSI). An HPLC (high-pressure liquid chromatography, LC-Forte/R, YMC, Japan) system equipped with a Luna C18 column (250 x 21.2 mm, Phenomenex Inc. USA) was used for the purification and purity tests at room temperature. The methods used in the purity test were as follows: (method A) eluent A: 0.1% TFA in water, B: 0.1% TFA in ACN; gradient: 5% B to 97% B in 20 min; flow rate 12 mL/min, (method B) eluent A: 10 mM ammonium acetate in water, B: 10 mM ammonium acetate in ACN ; gradient: 5% B to 40% B in 3 min, 40% B to 80% B in 25 min, 80% B to 100% B in 3 min; flow rate 12 mL/min. The purity of all products was determined using elemental analysis, or a reverse-phase HPLC with UV-vis detection at 320 nm.

Synthesis and Characterization.

2,3-Bis-*tert*-butoxycarbonylamino-propionic acid (1). The title compound was prepared according to the literature method with little modification.[22] Yield: 7.8 g (95%). ^{1}H NMR ($CDCl_3$): δ = 1.45 (*s*, 18H, CH_3), 3.55 (*m*, 2H, CH_2), 4.12 (*s*, 1H, CH), 4.27–5.17 (*m*, 1H, NH), 5.85 (*s*, 1H, OH), 2.05 (*s*, 1H, NH). Anal. Calcd for $C_{13}H_{24}O_6N_2 \cdot 2EtOAc$: C, 51.71; H, 8.04; N, 8.10. Found: C, 51.87; H, 8.15; N, 7.75.

[2-(4-Benzothiazol-2-ylphenylcarbamoyl)-2-*tert*-butoxycarbonylamino-ethyl]-carbamic acid *tert*-butyl ester (2). 2,3-Bis-*tert*-butoxycarbonylamino-propionic acid (7.00 g, 23.01 mmol) was dissolved in pyridine (40 ml) and benzothiazole aniline (BTA) (5.20 g, 23.01 mmol) in pyridine (20 ml) was added slowly. Resulting mixture stirred for 30 min and triphenyl phosphite (7.13 ml, 23.01 mmol) was added drop wise. The solution was stirred for 3 h at 80 °C and then overnight at RT. Solid obtained was filtered and washed with D.I water and acetone. Crude product was recrystallized in absolute acetonitrile. The desired product was obtained as white powder. Yield : 9.6 g (81.4%). ^{1}H NMR ($CDCl_3$): δ = 9.28 (*s*, 1H, NH) 8.06−8.01 (*m*, 3H, BTA), 7.89−7.85 (*d*, 1H, BTA), 7.68−7.64 (*d*, 2H, BTA), 7.49−7.44 (*t*, 1H, BTA), 7.38−7.33 (*t*, 1H, BTA), 5.97-5.93 (*s*, 2H, NH), 4.02−3.98 (*d*, 1H, CH), 3.57-3.41 (*m*, 2H, CH_2), 1.50-1.40 (*d*, 18H,CH_3). Anal. Calcd for $C_{26}H_{32}N_4O_5S$: C, 60.92; H, 6.29; N, 10.93; S, 6.26. Found: C, 60.55; H, 6.36; N, 10.60; S, 5.98. HR-FAB-MS (m/z) for $C_{26}H_{33}N_4O_5S$): calcd, 513.2172 $[M+H]^+$; found, 513.2170 $[M+H]^+$.

2,3-Diamoniumtrifluoroacetate-N-(4-benzothiazol-2-yl-phenyl)-propionamide (3). TFA (10 ml) was added drop wise into solution of **2** (1.5 g, 2.92 mmol) in CH_2Cl_2 at 0 °C. Resulting yellow solution was stirred until starting was consumed. Solvent was removed and Et_2O was added to obtain precipitate. The solid was filtered and washed three times with Et_2O then dried to give the title compound as a pale yellow solid in quantitative yield. Yield: 0.82 g (90%), ^{1}H NMR (MeOH-d_4): δ = 8.75 (*s*, 1H, NH), 8.01−7.99 (*d*, 2H, BTA), 7.9−7.89 (*d*, 2H, BTA), 7.82−7.78 (*d*, 2H, BTA), 7.45 (*t*, 1H, BTA), 7.35 (*t*, 1H, BTA), 4.43 (*t*, 1H, CH), 3.62−3.55 (d_d, 1H, CH_2), 3.51-3.44 (d_d, 2H, CH_2), 1.94 (*s*, 2H, NH). Anal. Calcd for $C_{16}H_{16}N_4OS \cdot 3CF_3COOH$: C, 40.37; H, 2.93; N, 8.56; S, 4.90. Found: C, 40.74; H, 2.68; N, 8.86; S, 5.26. HR-FAB-MS (m/z) for $C_{16}H_{17}N_4OS$: calcd, 313.1123 $[M+H]^+$; found, 313.1121 $[M+H]^+$.

{[1-(4-Benzothiazol-2-yl-phenylcarbamoyl)-2-(bis-*tert*-butoxycarbonylmethyl-amino)-ethyl]-*tert*-butoxycarbonylmethyl-amino}-acetic acid *tert*-butyl ester (4). Compound **3** (2 g, 3.70 mmol), N, N-diisopropylethylamine (7.66 mL, 59.2 mmol) and KI (1.84 g, 11.1 mmol) were dissolved in DMF (20 mL) and the solution warmed to 45 °C. *tert*-Butylbromoacetate (5.77 ml, 29.6 mmol) was added drop wise into this solution over 30 min. Resulting solution was stirred for 4 h at 110 °C and cooled to RT. The solvent was removed and the residue was partitioned between 10% $NaHCO_3$ and ethyl acetate. The aqueous layer was extracted three more times with EtOAc. Combined organic layer was then washed with brine and dried over Na_2SO_4. Evaporation gave a dark brown oil that was purified by column chromatography (silica, hexanes/EtOAc, 9:1). The desired product **4** was obtained as a light brown oily solid. Yield: 3.37 g (82%). ^{1}H NMR ($CDCl_3$): δ = 10.85 (*s*, 1H, NH), 8.08−8.01 (*m*, 3H, BTA), 7.91−7.82 (d_d, 3H, BTA), 7.47 (*t*, 1H, BTA), 7.36 (*t*, 1H, BTA), 3.75 (*t*, 1H, CH), 3.62−3.40 (*m*, 8H, CH_2-^{t}Bu), 3.04-2.96 (*dd*, 2H, CH_2), 1.46 (*s*, 36H, ^{t}Bu). Anal. Calcd for $C_{40}H_{56}N_4O_9S{\cdot}3H_2O$: C, 58.37; H, 7.59; N, 6.81; S, 3.90; Found: C, 58.61; H, 7.31; N, 6.46; S, 3.58. HR-FAB-MS (m/z) for $C_{40}H_{57}N_4O_9S$: calcd, 769.3846 $[M+H]^+$; found, 769.3842 $[M+H]^+$.

[{1-(4-Benzothiazol-2-yl-phenylcarbamoyl)-2-(bis-carboxymethyl-amino)-ethyl]-carboxymethyl-amino}-acetic acid] (L). Compound **4** (1.5 g, 1.95 mmol) was dissolved in ACN (30 mL) and conc. HCl (15 mL) was added at 0 °C. Resulting solution was stirred for 20 h. An additional portion of HCl (5 mL) was added and the solution was stirred for one more hour. The volume was reduced by approximately 75% by rotary evaporation. The residue was diluted with water (30 mL) and the pH was adjusted to 2 by the addition of sodium hydroxide. The white precipitate appears which was collected by filtration and washed with D.I Water (pH 2.0), ethyl acetate (30 mL), and ether (30 mL). The desired product, L was obtained as a white powder. The purity also confirmed using HPLC (method A) (Figure S10). Yield: 0.89 g (83%). ^{1}H NMR ($CDCl_3$): δ = 8.06−8.01 (*m*, 2H, BTA), 7.99−7.96 (*d*, 2H, BTA), 7.85−7.83 (*d*, 2H, BTA), 7.52-7.49 (*t*, 1H, BTA), 7.42−7.39 (*t*, 1H, BTA), 5.50-5.48 (*s*, 2H, OH), 4.02−3.98 (*d*, 1H, CH), 3.96−3.76 (*m*, 8H, CH_2), 3.57-3.41 (*m*, 2H, CH_2), Anal. Calcd for $C_{24}H_{24}N_4O_9S{\cdot}H_2O$: C, 51.24; H, 4.66; N, 9.96; S, 5.70. Found: C, 51.02; H, 4.65; N, 9.64; S, 5.54. HR-FAB-MS (m/z) for $C_{24}H_{25}N_4O_9S$: calcd, 545.1342 $[M+H]^+$; found, 545.1340 $[M+H]^+$.

[Mn(EDTA-BTA)(H_2O)]$^{2-}$. Compound L (1 g, 1.8 mmol) was dissolved in MeOH (30 mL) and the pH of the solution adjusted to pH 6 with NaOH (1.0 M), then the mixture changed to suspension including the off-white precipitation. To this mixture, $MnCl_2 \cdot 4H_2O$ (0.36 g, 1.8 mmol) in MeOH (3 mL) was slowly added and stirred at RT for overnight, during this time the mixture was re-adjusted to pH 6. The precipitate was filtered, washed with cold methanol and dried under vacuum. Which was dissolved in a minimum amount of water and more purified by flash column chromatography (C18, 95:5 to 85:15, water:MeOH) to yield a white solid. Further purification carried out using preparative HPLC (method B) and also purity was confirmed (Figure S11). Yield: 0.35g (32%). HR-FAB-MS (m/z) for $C_{24}H_{20}MnN_4O_9S$: calcd, 595.0331 [M]; Found: 595.0327 [M].

Transmetalation kinetics. This experiment was performed following published literature with a slight modification.[18] About 20 µL of a 50 mM MES (2-(N-morpholino)ethanesulfonic acid)-buffered solution (pH 6.0) of $ZnCl_2$ was added to 1 mL of a buffered solution of 1 mM metal complex. The mixture was shaken briefly, and immediately used for measuring solvent T2 as a function of time. Control studies were also conducted with MnDPDP (Teslascan), Gd-DTPA (Magnevist), and Mn-EDTA for comparison. The measurements were performed on a 3 Tesla (T) whole body system (Discovery MR750w 3.0T, GE healthcare) at room temperature. The graph was plotted using the equation $\Delta R2(t) = R2(t) - R2(0)$, as function of time.

Relaxivity. Using an inversion recovery method, T1 measurements were made with a variable inversion time (TI) at 1.5T (64MHz, GE Healthcare Milwaukee, WI, USA). Magnetic resonance (MR) images were acquired at 35 different TI values over the frequency range 50 to 1750 msec. T1 relaxation times were achieved from the non-linear least square fit of the signal intensity measured at each TI value. In place of T2 measurements, the CPMG (Carr-Purcell-Meiboon-Gill) pulse sequence ware adapted for multiple spin-echo measurements. Thirty-four images were achieved with 34 different echo time (TE) values ranging from 10 to 1900 msec. T2 relaxation times were attained from the non-linear least squares fit of the mean pixel values of multiple spin-echo measurements at each

echo time. Relaxivities (R1 and R2) were then measured as an inverse of relaxation time per mM. The determined relaxation times (T1 and T2) and relaxivities (R1 and R2) were finally image-processed to provide the relaxation time map and relaxivity map, respectively.

Octanol-water partition coefficients. This experiment was performed following published literature.[29] Manganese(II) complex (1 mg) was dissolved in 2 mL of a 1:1 mixture of water and 1-octanol. The solution was shaken for 30 s, then the vial containing the mixture was placed on a rotator for gentle mixing to equilibrate for 48 h. The sample was then allowed to settle at room temperature for 24 h. Mn(II) concentrations of each layer were determined by ICP-MS (Inductively Coupled Plasma Mass Spectrometry). Partition coefficients were calculated from the equation log P = log (C_o/C_w), where log P is the logarithm of the partition coefficient, C_o is the concentration of Mn in the 1-octanol layer, and C_w is the concentration of Mn in the water layer.

Determination of binding constants. The binding constants of several CAs with HSA were measured following published literature.[26,27] The non-linear increase of the proton paramagnetic relaxation rates measured at 64 MHz in solutions containing 0.67 mM HSA, were fitted using equation 2, where K_a is the binding constant of the interaction with HSA, p^0 is the concentration of the HSA, s^0 is the paramagnetic complex concentration, N is the number of independent interaction sites (N was set to 1), and r_1^c and r_1^f are the relaxivities of the complex HSA-contrast agent and of the free contrast agent, respectively.

$$R_1^{p^{obs}} = 1000 \times \left\{ \left(r_1^f \times s^0\right) + \frac{1}{2}\left(r_1^c - r_1^f\right)\left((N \times p^0) + s^0 + K_a^{-1} - \sqrt{\left((N \times p^0) + s^0 + K_a^{-1}\right)^2 - 4 \times N \times s^0 \times p^0} \right) \right\} \quad (1)$$

Cell culture. The culture medium consisted of Dulbecco's Modified Eagle's Medium (DMEM, Gibco Invitrogen, Carlsbad, CA) or Roswell Park Memorial Institute (RPMI, Gibco Invitrogen, Carlsbad, CA), 10% (v/v) fetal bovine serum (FBS), and 1% (v/v) penicillin-streptomycin. Cells were

plated at a density of 2×10^5 cells/35 mm dish, incubated overnight for stabilization and then treated with Mn for 24 h in serum-depleted media.

Liver tumor model. An orthotopic xenograft mouse liver tumor model was approved by the Institutional Animal Care and Use of Committee of Daegu-Gyeongbuk Medical Innovation Foundation (DGMIF). Five-week-old male nude mice (BALB/c *nu/nu*) were purchased from Orient Bio (Seongnam, Korea) and housed in a specific pathogen-free facility at the Laboratory Animal Center of DGMIF before use. The mice were inoculated with HepG2-luc2 cells (1×10^6 cells in 50 μl HBSS) in the subcapsular parenchyma of the left liver lobe. The HepG2-luc2 cell line was purchased from Perkin Elmer Inc. Four weeks after inoculation, mice were imaged by the IVIS system to check tumor induction (Figure S11 in Supporting Information).

Bioluminescence imaging. Bioluminescence images were acquired using the IVIS Lumina system (Perkin Elmer). Mice were intraperitoneally administered firefly D-Luciferin potassium salt (Perkin Elmer) at a dose of 150 mg/kg body weight in Dulbecco's phosphate-buffered saline. During image acquisition, anesthesia was maintained with 2% isoflurane. Analysis was performed with Living Image® software by measuring the photon flux (measured in photons / [sec • cm^2 • steradian]) using a region of interest manually drawn over the body of the mouse. Signals were measured for approximately 1 h.

Cell viability assay (*in vitro* growth inhibition). Human prostate cancer cell line DU 145, and mouse liver cell line NCTC 1469 were plated at a density of 1×10^4 in 96-well plates. The DMEM or RPMI growth medium was removed and the cells were incubated with Gd-DTPA or Mn-EDTA-BTA in DMEM or RPMI serum-depleted medium for 24 h. Cell viability was assessed using the CCK-8 kit (Dojindo, Sunnyvale, CA) according to the manufacturer's protocol. In brief, 10 μL of CCK-8 solution was added to each well and the samples were incubated for 4 h before the absorbance was measured at 450 nm.

Cell fractions for MRI. NCTC 1469 cells were plated at a density of 2×10^5 in 35 mm dishes. The DMEM growth medium was removed, and the cells were incubated with Mn-EDTA-BTA (100 μM) in DMEM serum-depleted media for 12 h. The cells were washed with phosphate buffered saline (PBS) and harvested. For cell fractionation, cancer cells were lysed with three cycles of freezing and thawing in PBS, and lysates centrifuged at 1000 rpm for 5 min at 4 °C. The supernatant was the cytosolic fraction, and the first pellet was re-suspended in radioimmunoprecipitation assay (RIPA) buffer for 1 h at 4 °C and centrifuged at 12,000 rpm for 10 min at 4 °C. The supernatant corresponded to RIPA buffer-soluble membrane fraction and the final pellet contained nuclei and cell organelles. Collected cells were subject to MRI using a 1.5T MRI scanner.

***In vitro* MRI.** *In vitro* MR images were obtained with a 1.5 T (T) MR unit (GE Healthcare, Milwaukee, WI, USA) equipped with a homemade small animal RF coil. The imaging parameters for SE (Spin Echo) were as follows: repetition time (TR) = 500 ms; echo time (TE) = 13.6 ms; 10 mm field of view (FOV); 192 × 128 matrix size; 1.0 mm slice thickness; number of acquisition (NEX) = 15.

***In vivo* MRI.** All animal experiments were approved by and performed in accordance with the rules of, Kyungpook National University animal care committee. Six-week-old male ICR mice weighing 25-30 g were used for the MRI study. The mice were anesthetized with 1.5% isoflurane in oxygen. Measurements were made before and after tail vein injection of paramagnetic complexes. After each measurement, the mice were revived from anesthesia and placed in cages with free access to food and water. During these measurements, the animals were maintained at room temperature. Whole body MR images were obtained with a 1.5 T MR unit (GE healthcare) equipped with a homemade small animal RF coil. The coil was of receiver type bird cage with an inner diameter of 50 mm. The imaging parameters for spin echo (SE) T1-weighted images were as follows: repetition time (TR) = 300 ms; echo time (TE) = 12 ms; 11 mm field of view (FOV); 192 x 128 matrix size; 1.2 mm

slice thickness; number of acquisition (NEX) = 8. The imaging parameters for fast spin echo (FSE) T2-weighted images were as follows: TR = 2000 ms; TE = 40 ms; 11 mm FOV; 192 x 128 matrix size; 1.2 mm slice thickness; NEX = 8.

Image analysis. Anatomical positions with enhanced contrast were identified with respect to heart, liver, gallbladder, kidney, and bladder on post-contrast MR images. For quantitative measurement, signal intensities in specific regions of interest (ROI) were measured using the image processing program Image J (National Institutes of Health, USA). The CNR (contrast-to-noise ratio) was calculated using equation 1, where SNR is the signal to noise ratio.

$$CNR = SNR_{post} - SNR_{pre} \quad (2)$$

Biodistribution. Mn-EDTA-BTA was administered intravenously as a bolus (0.05 mmol/kg) via tail veins of four normal male mice (ICR mice; 25-30 g) for each time point. The mice were anesthetized and killed by exsanguination from the vena cava at each time point (after 30 min, 1, 6, 12 and 24 h injection time). The Mn concentration was measured in various tissues (brain, heart, liver, gall bladder, spleen, intestine, bladder, kidney, blood, and lung) by digesting the tissues with HNO_3 (70%) and H_2O_2 (30%) at 180 ℃ for 3 h, and measuring the concentration in the clear diluted solution with an inductively coupled plasma spectrophotometer (ICP Spectrophotometer, Optima 7300DV, Perkin Elmer, USA). The detection limit of this method is 0.01 ppm.[30]

ASSOCIATED CONTENT

Supporting information

The Supporting Information is available free of charge on the ACS Publications website at DOI:

^{1}H NMR and HR-FAB-MS data of synthesized complexes, HPLC spectra of L and Mn-EDTA-BTA and bioimage of liver tumor model (PDF)

Molecular formula strings (CSV)

AUTHOR INFORMATION

Corresponding Authors

*For Y.C.: Phone, (+)82-53-420-5471; E-mail, ychang@knu.ac.kr

*For T.J.K.: Phone, (+)82-53-950-4127; E-mail, tjkim@knu.ac.kr

Notes

‡These authors contributed equally to the work.

*Authors to whom correspondence should be addressed.

Author Contributions

The manuscript was written through contributions of all authors. All authors have given approval to the final version of the manuscript. ‡These authors contributed equally to the work

ACKNOWLEDGMENTS

This work was supported by the Basic Research Laboratory (BRL) Program (2013R1A4A1069507) through the National Research Foundation funded by the Ministry of Science, ICT and Future Planning.

ABBREVIATIONS

EDTA, ethylenediaminetetraacetic acid; BTA, benzothiazole aniline; MRI, magnetic resonance imaging; MnDPDP, mangafodipir trisodium; NSF, nephrogenic systemic fibrosis; CA, contrast agent; Gd-DTPA, gadopentetic acid; HSA, human serum albumin; ICR, Institute of Cancer Research; CNR, contrast to noise ratio; Gd-EOB-DTPA, Gadoxetic acid; Gd-BOPTA, Gadobenic acid; RT, room temperature; HPLC, high pressure liquid chromatography; MES, (2-(N-morpholino)ethane sulfonic acid); Mn-EDTA, ethylenediaminetetraacetic acid manganese disodium salt hydrate; TI, inversion time; CPMG, Carr-Purcell-Meiboon-Gill pulse sequence; TE, echo time; TR, repetition time; SE, spin echo; FSE, fast spin echo; FOV, field of view; NEX, number of acquisition; ROI, regions of interest; DMEM, Dulbecco's Modified Eagle's Medium; RPMI, Roswell Park Memorial Institute; FBS, fetal bovine serum; HSA, human serum albumin; PBS, phosphate buffered saline; HBSS, Hank's Balanced Salt Solution; IVIS, in vivo imaging instruments; RIPA, radioimmunoprecipitation assay; CCK-8, cell counting kit-8.

REFERENCES

(1) Wendland, M. F. Applications of manganese-enhanced magnetic resonance imaging (MEMRI) to imaging of the heart. *NMR Biomed*. **2004,** *17*, 581-594.

(2) Mendonca-Dias, M. H.; Gaggelli, E.; Lauterbur, P. C. Paramagnetic contrast agents in nuclear magnetic resonance medical imaging. *Semin. Nucl. Med*. **1983**, *13*, 364-376.

(3) Geraldesa, C.; Laurent, S. Classification and basic properties of contrast agents for magnetic resonance imaging. *Contrast Media Mol. Imaging* **2009**, *4*, 1–23.

(4) Grobner, T. Gadolinium – a specific trigger for the development of nephrogenic fibrosing dermopathy and nephrogenic systemic fibrosis? *Nephrol. Dial. Transplant.* **2006**, *21*, 1104–1108.

(5) Marckmann, P.; Skov, L.; Rossen, K.; Dupont, A.; Damholt, M. B.; Heaf, J. G.; Thomsen, H. S. Nephrogenic systemic fibrosis: suspected causative role of gadodiamide used for contrast-enhanced magnetic resonance imaging. *J. Am. Soc. Nephrol.* **2006***, 17*, 2359–2362.

(6) Kanda, T.; Fukusato, T.; Matsuda, M.; Toyoda, K.; Oba, H.; Kotoku, J.; Haruyama, T.; Kitajima, K.; Furui, S. Gadolinium-based contrast agent accumulates in the brain even in subjects without severe renal dysfunction: evaluation of autopsy brain specimens with inductively coupled plasma mass spectroscopy. *Radiology* **2015**, *276*, 228–232.

(7) Kueny-Stotz, M.; Garofalo, A.; Felder-Flesch, D. Manganese-enhanced MRI contrast agents: from small chelates to nanosized hybrids. *Eur. J. Inorg. Chem.* **2012**, *12*, 1987–2005.

(8) Drahoš, B; Lukeš, I.; Tóth, É. Manganese (II) complexes as potential contrast agents for MRI. *Eur. J. Inorg. Chem*. **2012**, *12*, 1975–1986.

(9) Porcheron, G.: Garenaux, A.: Proulx, J.; Sabri, M.; Dozois, C. M. Iron, copper, zinc, and manganese transport and regulation in pathogenic enterobacteria: correlations between strains, site of infection and the relative importance of the different metal transport systems for virulence. *Front. Cell. Infect. Microbiol.* **2013**, *3*, 1-24.

(10) Brurok, H.; Skoglund, T.; Berg, K.; Skarra, S.; Karlsson, J. O. G.; Jynge, P. Myocardial manganese elevation and proton relaxivity enhancement with manganese dipyridoxyl diphosphate. Ex vivo assessments in normally perfused and ischemic guinea pig hearts. *NMR Biomed.* **1999**, *12*, 364-372.

(11) Pan, D.; Schmieder, A. H.; Wickline, S. A.; Lanza G. M. Manganese-based MRI contrast agents: past, present, and future. *Tetrahedron* **2011**, *67*, 8431-8444.

(12) Cersosimo, M. G.; Koller, W.C. The diagnosis of manganese-induced parkinsonism. *Neuro Toxicology* **2006**, *27*, 340–346.

(13) Bock, N. A.; Silva, A. C. Manganese: a unique neuroimaging contrast agent. *Future Neurol*. **2007**, *2*, 297–305.

(14) Ni, Y.; Marchal, G. Clinical implications of studies with MnDPDP in animal models of hepatic abnormalities. *Acta Radiologica* **1997**, *38*, 724-731.

(15) Karlsson, J. O. G.; Ignarro, L. J.; Lundström, I.; Jynge, P.; Almén, T. Calmangafodipir [$Ca_4Mn(DPDP)_5$], mangafodipir (MnDPDP) and MnPLED with special reference to their SOD mimetic and therapeutic properties. *Drug Discovery Today* **2015**, *20*, 411-421.

(16) Rocklage, S. M.; Cacheris, W. P.; Quay, S. C.; Hahn, F. E.; Raymond, K. N. Manganese(II) N,N'-dipyridoxylethylenediamine-N,N'-diacetate 5,5'-bis(phosphate). Synthesis and characterization of a paramagnetic chelate for magnetic resonance imaging enhancement. *Inorg. Chem.* **1989**, *28*, 477-485.

(17) Zheng, W.; O'Neal, S. L. Manganese toxicity upon overexposure: a decade in review. *Curr. Environ. Health Rep.* **2015**, *2*, 315-328.

(18) Caravan, P.; Gale, E. M.; Atanasova, I. P.; Blasi, F.; Ay, I. A Manganese alternative to gadolinium for MRI contrast. *J. Am. Chem. Soc*. **2015**, *137*, 15548.

(19) Baroni, S.; Serra, S. C.; Mingo, A. F.; Lux, G.; Giovenzana, G. B.; Lattuada, L. Synthesis and relaxometric characterization of a new Mn(II)-EDTA-deoxycholic acid conjugate complex as a potential MRI blood pool agent. *Chemistry Select* **2016**, *1*, 1607 – 1612.

(20) Nam, K.; Jung, K.; Chang, Y.; Kim, T. Gadolinium complex of 1,4,7,10-tetraazacyclododecane-1,4,7-trisacetic acid (DO3A) conjugate of [(p-aniline benzothiazole)methyl] pyridine as a tumor-targeting MRI contrast agent. *Bull. Korean Chem. Soc*. **2013**, 34(12), 3654-3658.

(21) Van Beers, B. E.; Pastor, C. M.; Hussain, H. K. Primovist, Eovist: what to expect? *J. Hepatol*. **2012**, 57(2), 421-429.

(22) Moradell, S.; Lorenzo, J.; Rovira, A.; Zutphen, S.; Aviles, F. X.; Moreno, V.; Llorens, R.; Martinez, M. A.; Reedijk, J.; Llobet, A. Water-soluble platinum(II) complexes of diamine chelating ligands bearing amino-acid type substituents: the effect of the linked amino acid and the diamine chelate ring size on antitumor activity, and interactions with 5'-GMP and DNA, *J. Inorg. Biochem*. **2004**, *98*, 1933-1946.

(23) Troughton, J. S.; Greenfield, M. T.; Greenwood, J. M.; Dumas, S.; Wiethoff, A. J.; Wang, J.; Spiller, M.; McMurry, T. J.; Caravan, P. Synthesis and evaluation of a high relaxivity manganese(II)-based MRI contrast agent. *Inorg. Chem.* **2004**, *43*, 6313-6323.

(24) Muller, R. N.; Laurent, S.; Elst, L. V.; Copoix, F. Stability of MRI paramagnetic contrast media: a proton relaxometric protocol for transmetallation assessment. *Invest. Radiol*. **2001**, *36*, 115-122.

(25) Kim, H.-K.; Park, J.-A.; Kim, K. M.; Sk, Md. N.; Kang, D.-S.; Lee, J.; Chang, Y.; Kim, T.-J. Gd-complexes of macrocyclic DTPA conjugates of 1,10-bis(amino)ferrocenes as high relaxivity MRI blood-pool contrast agents (BPCAs). *Chem. Commun.* **2010**, *46*, 8442- 8444.

(26) Muller, R. N.; Raduchel, B.; Laurent, S.; Platzek, J.; Pierart, C.; Mareski, P.; Elst, L. V. Physicochemical characterization of MS-325, a new gadolinium complex, by multinuclear relaxometry. *Eur. J. Inorg. Chem.* **1999**, *11*, 1949-1955.

(27) Chang, Y.; Kim, T.-J.; Kim, H.-K.; Kang M.-K.; Jung, K.-H.; Kang S.-H.; Kim Y.-H.; Jung J.-C.; Lee, G.-H. Gadolinium complex of DO3A-benzothiazole aniline (BTA) conjugate as a theranostic agent. *J. Med. Chem*. **2013**, *56*, 8104-8111.

(28) Chabanova, E.; Logager, V. B.; Moller, J. M.; Thomsen, H. S. Manganese based MR contrast agents: formulation and clinical applications. *The Open Drug Safety Journal* **2011**, *2*, 29-38.

(29) Meade, T. J.; MacRenaris, K. W.; Ma, Z.; Krueger, R. L.; Carney, C. E. Cell-permeable esterase-activated Ca(II)-sensitive MRI contrast agent. *Bioconjugate Chem*. **2016**, *27*, 465-473.

(30) Lokling, K. E.; Fossheim, S. L.; Klaveness, J.; Skurtveit, R. Biodistribution of pH-responsive liposomes for MRI and a novel approach to improve the pH-responsiveness. *J. Controlled Release* **2004**, *98*, 87−95.

(31) Jung, K.-H.; Kim, H.-K.; Lee, G. H.; Kang, D.-S.; Park, J.-A.; Kim, K. M.; Chang, Y.; Kim, T.-J. Gd complexes of macrocyclic diethylenetriaminepentaacetic acid (DTPA)

biphenyl-2,2‘-bisamides as strong blood-pool magnetic resonance imaging contrast agents. *J. Med. Chem*. **2011**, *54*, 5385-5394.

Table 1. Relaxivity and octanol-water partition coefficients data of Mn-EDTA-BTA, Mn-EDTA, MnDPDP and Gd-DTPA in water (64 MHz, 297 K).

	r_1 ($mM^{-1}sec^{-1}$)		r_2 ($mM^{-1}sec^{-1}$)		$logP_{oct/wat}$
	water	**HSA[c]**	**water**	**HSA[c]**	
Mn-EDTA-BTA	3.5±0.1	15.1±1.9	4.9±0.1	34.5±3.9	-1.84
Mn-EDTA	1.9±0.1	-	3.7±0.1	-	-2.72
MnDPDP[a]	2.8	-	3.7	-	-3.07
Gd-DTPA[b]	3.3	4.3	3.9	4.4	-3.16

[a]Data obtained from ref 7, [b]Data obtained from ref 31. [C][HSA] = 0.67mM in water.

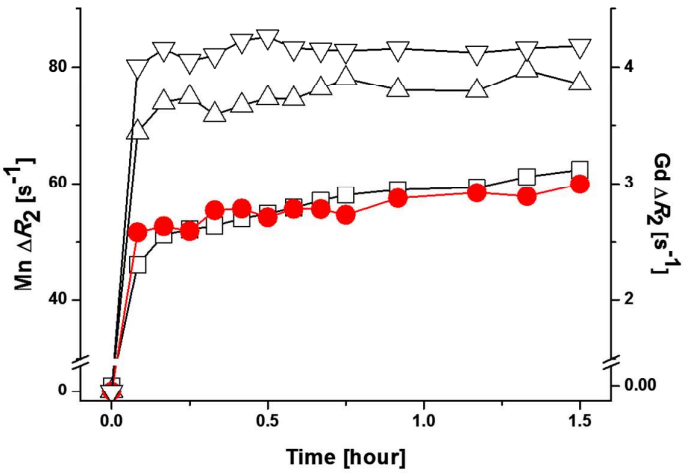

Figure 1. Transmetalation of 1 mM MnDPDP (△), Mn-EDTA (▽), Gd-DTPA (□) and Mn-EDTA-BTA (●) by 10 mM Zn^{2+} plotted by ΔR_2 as a function of time at 3T and 293 K. ($\Delta R_2(t) = R_2(t) - R_2(0)$).

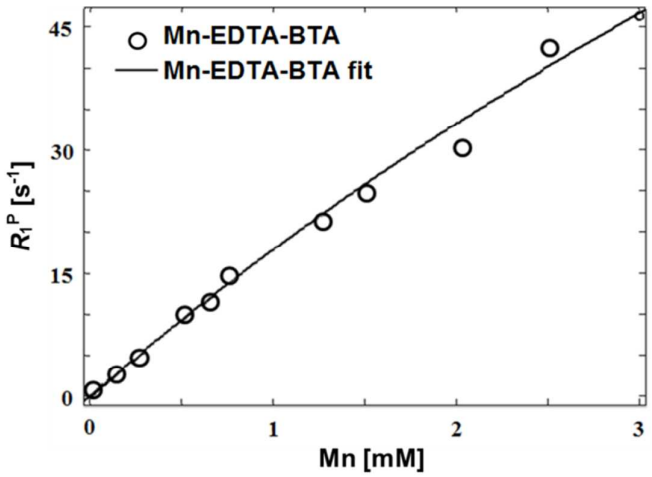

Figure 2. Proton longitudinal paramagnetic relaxation rates of Mn-EDTA-BTA as a function of [Mn] in aqueous solution of HSA (0.67 mM) at 64 MHz and 293 K, fitted using eq. 1.

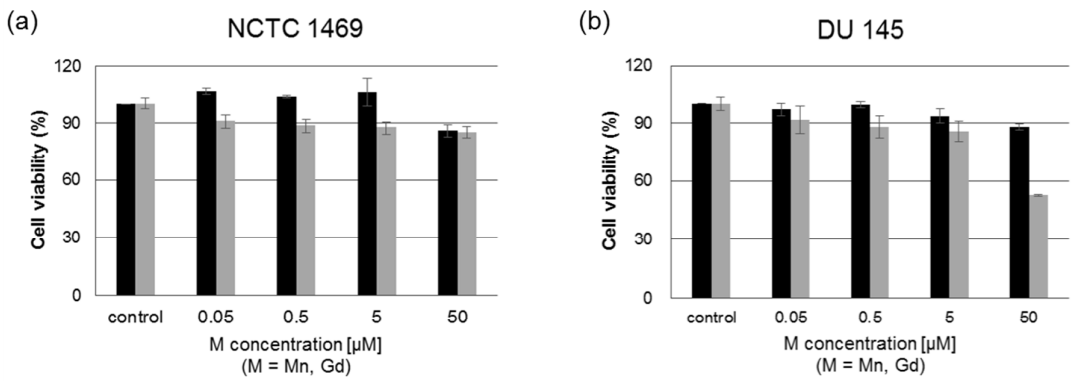

Figure 3. Relative proliferation (%) of (a) mouse liver cells (NCTC 1469) and (b) the human prostate cancer cells (DU 145) after treatment with various concentrations of Mn-EDTA-BTA (black bars) or Gd-DTPA (gray bars).

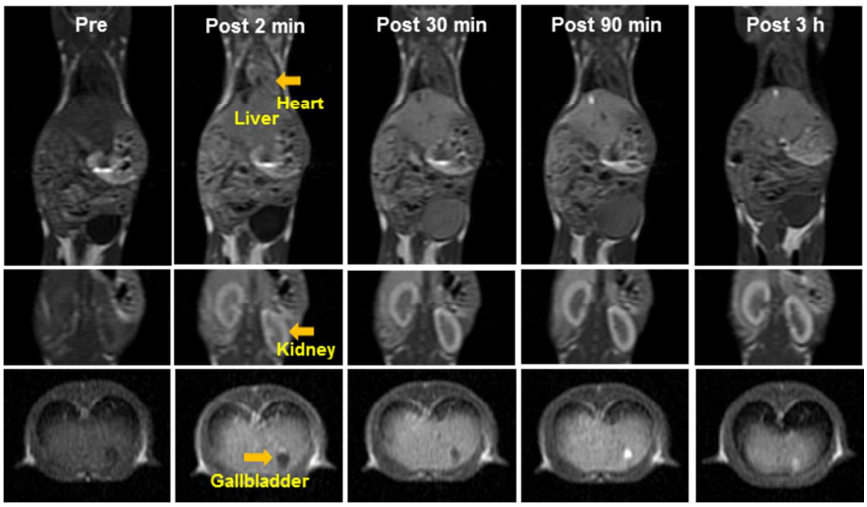

Figure 4. *In vivo* T1-weighted spin echo (SE) MR images of normal ICR mice obtained after tail vein injection of Mn-EDTA-BTA (0.05 mmol/kg).

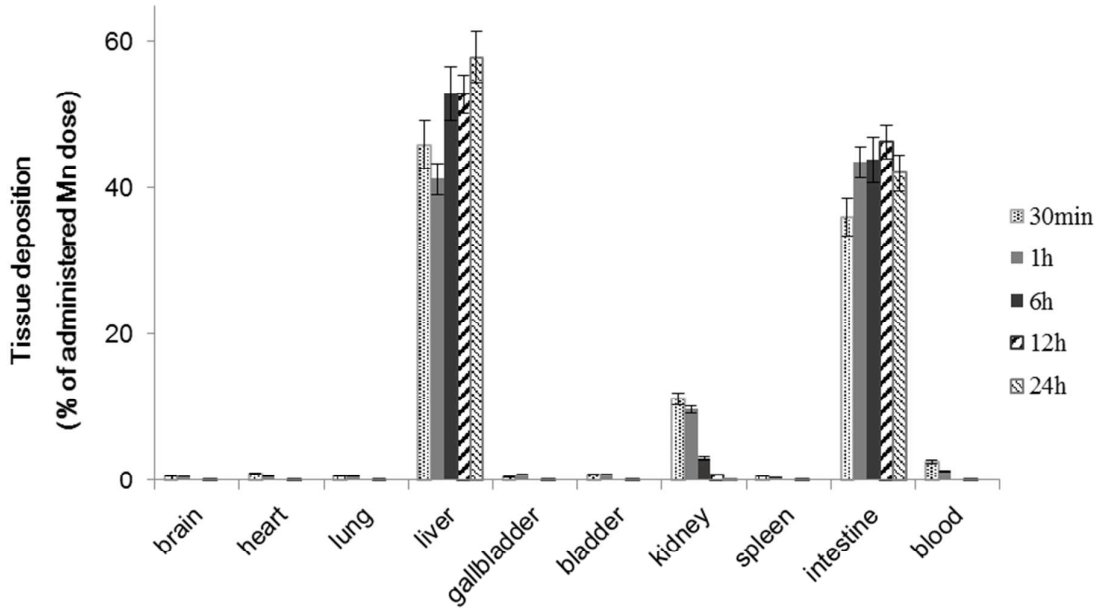

Figure 5. Biodistribution of Mn-EDTA-BTA (0.05 mmol Mn/kg body weight) in normal ICR mice represented by Mn percentage in each tissue. Groups of mice (n = 4) were sacrificed at 30 min, 1 h, 6 h, 12 h, and 24 h.

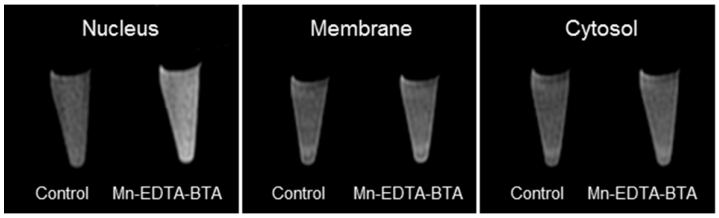

Figure 6. T_1-weighted MR images of NCTC-1469 cell fractions incubated with Mn-EDTA-BTA (100μM) for 12h.

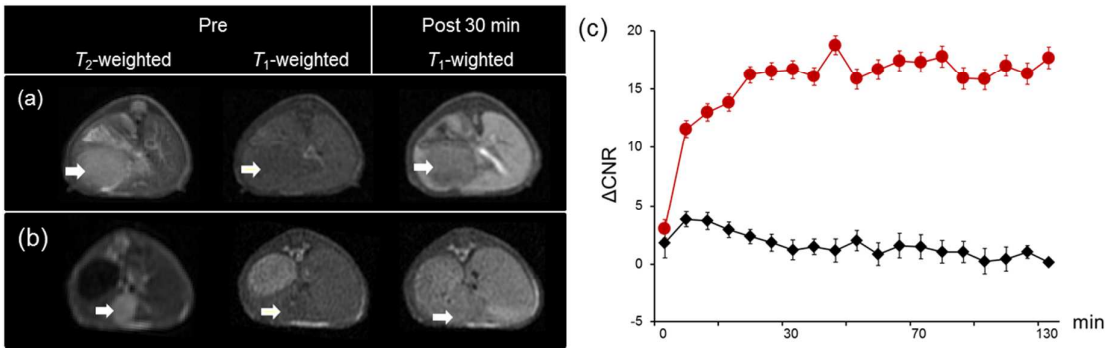

Figure 7. Axial T2-weighted and T1-weighted MR images of HepG2 xenograft mice. (a) before injection and 30 min after injection with Mn-EDTA-BTA (0.05 mmol/kg) and (b) before injection and 30 min after injection with MnDPDP (0.01 mmol/kg). The white arrows show the liver tumor lesion. (C) The difference of CNR between normal and tumor liver tissue as a function of time. CNR was measured in T1-weighted images. Mn-EDTA-BTA (filled squares) and MnDPDP (filled circles).

Scheme 1. Synthesis of Mn-EDTA-BTA

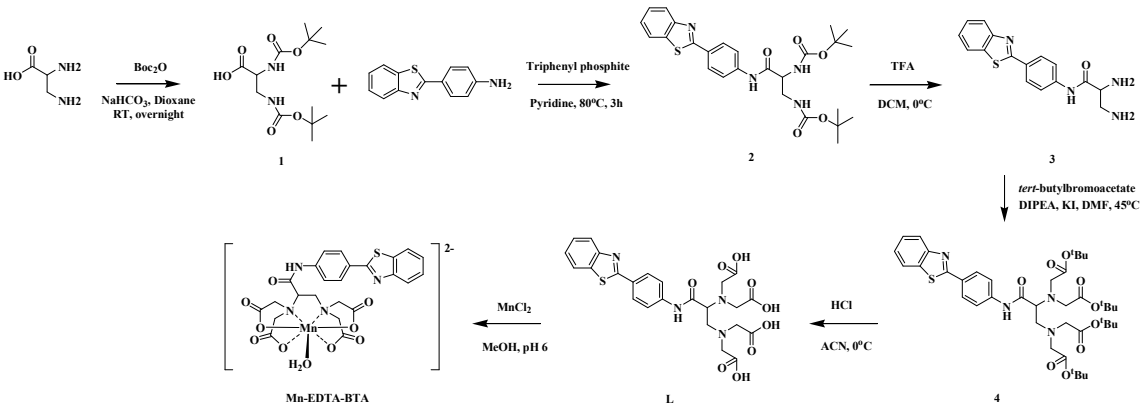

Table of Contents graphic